ЯДЕРНА ФІЗИКА
NUCLEAR PHYSICS

УДК 539.142 https://doi.org/10.15407/jnpae2020.03.223

S. V. Lukyanov*, A. I. Sanzhur

Institute for Nuclear Research, National Academy of Sciences of Ukraine, Kyiv, Ukraine

*Corresponding author: lukyanov@kinr.kiev.ua

INFLUENCE OF SURFACE EFFECTS ON NEUTRON SKIN IN ATOMIC NUCLEI

The influence of the diffuse surface layer of a finite nucleus on the mean square radii and their isotopic shift is investigated. We present the calculations within the Gibbs - Tolman approach using the experimental values of the nucleon separation energies. Results are compared with that obtained by means of a direct variational method based on Fermi-like trial functions.

Keywords: neutron skin, Gibbs - Tolman approach, direct variational method, Skyrme forces.

1. Introduction

The finite nucleus possesses the surface diffuse layer due to the quantum penetration of particles into the classically forbidden region. As a result, there is ambiguity in the determination of the nuclear size [1]. Information on the size of atomic nuclei and average characteristics of radial nucleon distributions can be obtained from the values of mean square radii of nuclei [2]. In the analysis of experimental data, the two-parameter Fermi function is often used for the spatial distribution of nucleons,

$$F_q(r) = \left[1 + \exp\left(\frac{r - R_q}{a_q}\right)\right]^{-1}, \qquad (1)$$

where R_q is the half-density radius and a_q is the diffuseness parameter of the distribution. Here, $q = n$ is for neutron and $q = p$ for proton distribution. For a two-component system, two different patterns may arise [3] depending on the parameter values R_q and a_q. For the same values of the diffuseness, $a_n = a_p$, but for different values of radii, $R_n > R_p$, one considers neutron skin. In the opposite case of the same values of the radii, $R_n = R_p$, and for different values of the diffuseness parameter, $a_n > a_p$, there is a neutron halo. Studies show the mixture of two mentioned patterns with approximately equal contributions [4].

In this paper, the effect of the diffuse surface layer of a nucleus on the mean square radii is considered making the comparison between the results of two models. First, we adopt the spatial distribution of nucleons having a sharp boundary at the equimolar radius. Within the Gibbs - Tolman (GT) approach [5 - 8] the values of the equimolar radius and the bulk nucleon density are obtained using the experimental data on nucleon separation energies. Second, we consider the diffuse spatial distribution of nucleons in a nucleus. We apply the direct variational method based on the specific Fermi-like trial functions [4, 9, 10] and the bulk nucleon density is normalized to that obtained using the GT approach. The comparison of the two above mentioned considerations allow us to allocate the effects of the surface layer on rms radii and their isotopic shift. Sec. 2 gives the basics of the Gibbs - Tolman approach and direct variational method. Results and discussion are presented in Sec. 3, conclusions are summarized in Sec. 4.

2. The model

2.1. The Gibbs - Tolman approach

Following the Gibbs - Tolman approach, we consider the spatial distribution of nucleons in the spherical nucleus having a sharp boundary located within the surface region. The dividing spherical surface of the radius R separates the nucleus into bulk and surface parts with the corresponding volume $V = 4\pi R^3/3$ and surface area $S = 4\pi R^2$. The total energy E of the nucleus is also divided into the volume, E_V, and, the surface, E_S, parts, respectively. Namely,

$$E = E_V + E_S + E_C. \qquad (2)$$

Here the Coulomb energy E_C is fixed and does not depend on the dividing radius R. The volume energy E_V is considered as the energy of homogeneous nuclear matter $E_V = E_\infty$ contained in the volume V.

We consider the two-component nuclear matter with the neutron-proton asymmetry parameter $X = (N - Z)/A$ where N and Z are, respectively

the neutron and proton numbers, $A = N + Z$ is the mass number. The neutron, μ_n, and proton, μ_p, chemical potentials are defined as

$$\mu_n = \left.\frac{\partial E_V}{\partial N}\right|_Z, \quad \mu_p = \left.\frac{\partial E_V}{\partial Z}\right|_N. \tag{3}$$

By the assumption of the GT approach, the nuclear matter inside a certain volume is taken to be in a state having the same values of chemical potentials as those of the real nucleus (see [9])

$$\mu_q(\{\rho_{q,V}\}) = -s_q - \lambda_{q,C}, \tag{4}$$

where s_q is the single-nucleon separation energy, $\rho_{q,V}$ is the bulk nuclear matter density of the step r-distribution

$$\rho_q(r) = \rho_{q,V}\,\Theta(R_{s,q} - r), \tag{5}$$

where $R_{s,q}$ are the partial (neutron and/or proton) radii. The Coulomb contribution $\lambda_{q,C}$ to the chemical potential $\lambda_q = -s_q$ of the nucleus is subtracted in Eq. (4) since the resulting value μ_q of Eq. (3) corresponds to uncharged nuclear matter. The value of Coulomb contribution in (4) is determined by

$$\lambda_{n,C} = \left.\frac{\partial E_C}{\partial N}\right|_Z, \quad \lambda_{p,C} = \left.\frac{\partial E_C}{\partial Z}\right|_N. \tag{6}$$

Below we will approximate the Coulomb energy $E_C(X)$ by the smooth function

$$E_C(X) = e_C(A)(1-X)^2 A, \tag{7}$$

where

$$e_C(A) = 0.207A^{2/3} - 0.174A^{1/3}$$

is the Coulomb energy parameter estimated from the fit to the experimental data, see [11].

Considering the asymmetric nuclear matter with the asymmetry parameter $X \gg 1$, the bulk energy per particle can be used as [9]

$$E_V / A \equiv e_0(\rho_V) + e_2(\rho_V)\left(\frac{\rho_{-,V}}{\rho_V}\right)^2, \tag{8}$$

where

$$e_0(\rho_V) = \frac{\hbar^2}{2m}\alpha\rho_V^{2/3} + \frac{3t_0}{8}\rho_V + \frac{t_3}{16}\rho_V^{\nu+1} + \frac{\alpha}{16}\left[3t_1 + t_2(5+4x_2)\right]\rho_V^{5/3} \tag{9}$$

and

$$e_2(\rho_V) = \frac{5}{9}\frac{\hbar^2}{2m}\alpha\rho_V^{2/3} - \frac{t_0}{8}(1+2x_0)\rho_V - \frac{t_3}{48}(1+2x_3)\rho_V^{\nu+1} + \frac{5\alpha}{72}\left(t_2(4+5x_2) - 3t_1x_1\right)\rho_V^{5/3}. \tag{10}$$

Here $\alpha = (3/5)(3\pi^2/2)^{2/3}$, $\rho_V = \rho_{n,V} + \rho_{p,V}$ and $\rho_{-,V} = \rho_{n,V} - \rho_{p,V}$ are the total nucleon and the neutron excess bulk densities, respectively, t_i, x_i and ν are the parameters of Skyrme force.

The surface energy is given by [9]

$$E_S = (\sigma + \mu\rho_S + \mu_-\rho_{-,S})S, \tag{11}$$

where σ is the surface tension coefficient. Here $\mu = (\mu_n + \mu_p)/2$ and $\mu_- = (\mu_n - \mu_p)/2$ are, respectively, the isoscalar and isovector chemical potentials, $\rho_S = (\rho_{n,S} + \rho_{p,S})/2$ is the isoscalar surface density, and $\rho_{-,S} = (\rho_{n,S} - \rho_{p,S})/2$ is the isovector surface density (see details in Ref. [9]).

In accordance with the GT concept, the actual equimolar radius R_e of the droplet is determined by the requirement that the contribution to E_S from the bulk terms of Eq. (11) should be excluded. This requirement can be satisfied if the following condition is fulfilled:

$$\left(\mu\rho_S + \mu_-\rho_{-,S}\right)_{R=R_e} = 0. \tag{12}$$

Eq. (12) determines the equimolar radius R_e.

As soon as the chemical potentials of a nucleus is known, one obtains the partial volume densities $\rho_{q,V}$ using Eqs. (3) - (10). Then, calculating the partial surface densities

$$\rho_{n,S}[R] = \frac{N}{4\pi R^2} - \frac{1}{3}\rho_{n,V}R,$$

$$\rho_{p,S}[R] = \frac{Z}{4\pi R^2} - \frac{1}{3}\rho_{p,V}R \tag{13}$$

and applying the condition (see also Eq. (12))

$$\rho_{q,S}[R_{q,e}] = 0, \tag{14}$$

one finds the partial equimolar radii $R_{q,e}$ [9]. The root mean square (rms) radius for the nucleon density distribution $\rho_q(\mathbf{r})$ is defined as

$$\sqrt{\langle r_q^2\rangle} = \sqrt{\int d\mathbf{r}\, r^2\rho_q(\mathbf{r}) \Big/ \int d\mathbf{r}\,\rho_q(\mathbf{r})}. \tag{15}$$

In particular, for the step distribution function (5), the corresponding rms radii are given by

$$\sqrt{\langle r_q^2 \rangle} = \sqrt{\frac{3}{5}} R_{q,e}. \tag{16}$$

2.2. The direct variational method

In order to consider the asymmetry of the diffuse surface of the spatial distribution of nucleons, according to the direct variational method (see, for example, [9, 12]), we adopt the trial function for $\rho_q(\mathbf{r})$ as a power of the Fermi function, namely

$$\rho_q(\mathbf{r}) = \rho_{0,q} F_q(r)^{\xi_q}, \tag{17}$$

where $\rho_{0,q}$, R_q, a_q and ξ_q are the variational parameters. The profile function $\rho_q(r)$ should satisfy the conservation conditions for numbers of neutrons and protons

$$\int d\mathbf{r}\rho_n(\mathbf{r}) = N, \quad \int d\mathbf{r}\rho_p(\mathbf{r}) = Z. \tag{18}$$

The total energy of a nucleus is given by

$$E_{\text{tot}} = E_{\text{kin}} + E_{\text{Sk}} + E_C, \tag{19}$$

where E_{kin} is the kinetic energy, E_{Sk} is the potential energy of the Skyrme interaction, and E_C is the Coulomb energy. In the case of finite nuclei, the kinetic energy is

$$E_{\text{kin}} = \int d\mathbf{r}\varepsilon_{\text{kin}}(\mathbf{r}), \tag{20}$$

where the kinetic energy density $\varepsilon_{\text{kin}}(\mathbf{r})$ is given by the sum of the neutron and proton contributions

$$\varepsilon_{\text{kin}}(\mathbf{r}) = \varepsilon_{\text{kin,n}}(\mathbf{r}) + \varepsilon_{\text{kin,p}}(\mathbf{r}). \tag{21}$$

We adopt the extended Thomas-Fermi approximation for the kinetic-energy density [13]

$$\varepsilon_{\text{kin,q}}(\mathbf{r}) = \frac{\hbar^2}{2m}\left[\frac{3}{5}\left(3\pi^2\right)^{2/3}\rho_q^{5/3} + \frac{1}{36}\frac{\left(\nabla\rho_q\right)^2}{\rho_q} + \frac{1}{3}\nabla^2\rho_q\right]. \tag{22}$$

In our consideration, the potential energy E_{Sk} also includes gradient terms due to the spin-orbit interaction. We note that pair interactions are not considered here.

For the ground state of the nucleus, the values of the variational parameters can be found by minimizing the total energy of the nucleus with respect to all possible small changes of the variational parameters, provided the conditions (18) are fulfilled. Below, in the subsequent calculations, the values of the nucleon density parameters $\rho_{0,q}$ will be normalized to the values obtained within the GT approach using the experimental data on the chemical potentials, see also Eq. (4),

$$\rho_{0,q} = \rho_{q,V}. \tag{23}$$

In view of Eqs. (17) and (18) the conditions for the particle number conservation are written by

$$\int d\mathbf{r}F_n(r)^{\xi_n} = \frac{N}{\rho_{n,V}}, \quad \int d\mathbf{r}F_p(r)^{\xi_p} = \frac{Z}{\rho_{p,V}}. \tag{24}$$

Thus, fixing the values of $\rho_{0,q}$ and R_q using the relations (23) and (24) the number of free variational parameters is reduced to four, that are a_q and ξ_q. For the trial functions are given by (17) one can obtain the leptodermous expansion ($a_q / R_q >> 1$) of the rms radius [4]:

$$\sqrt{\langle r^2 \rangle_q} \approx \sqrt{\frac{3}{5}} R_q \left\{1 + \kappa_0(\xi_q)\frac{a_q}{R_q} - \frac{7}{2}\left(\kappa_0^2(\xi_q) - 2\kappa_1(\xi_q)\right)\left(\frac{a_q}{R_q}\right)^2 + \frac{1}{6}\left(75\kappa_0^3(\xi_q) - 204\kappa_0(\xi_q)\kappa_1(\xi_q) + 81\kappa_2(\xi_q)\right)\left(\frac{a_q}{R_q}\right)^3\right\}, \tag{25}$$

where the coefficients $\kappa_j(\xi)$ are the generalized Fermi integrals,

$$\kappa_j(\xi) = \int_0^\infty dx\, x^j \left[(1+e^x)^{-\xi} - (-1)^j\left(1-(1+e^{-x})^{-\xi}\right)\right]. \tag{26}$$

3. Numerical calculations

Here we present the results of numerical calculations for the neutron and proton rms radii for isotopes of sodium, tin, and lead. The SkM* parameterization [13] for the Skyrme nucleon-nucleon interaction was used in the calculations. Since sodium isotopes $^{21\text{-}24,28\text{-}21}$Na have the observed prolate deformation [14], we will consider the effective rms radii. Fig. 1 shows the calculation results for the effective rms radii of the proton spatial distributions in sodium isotopes versus the mass number *A*.

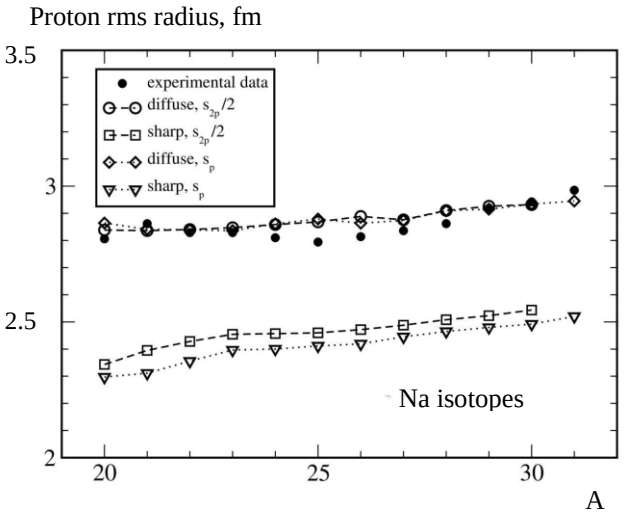

Fig. 1. Dependence of the effective rms radii for proton spatial distributions in Na isotopes on the mass number A. The black circles are the experimental data [14], the triangles are the calculations within the GT approach using one-proton separation energy; the rhombuses are the calculations for the diffuse distribution with one-proton separation energy; the squares are the calculations in the framework of the GT approach, half of the two-proton separation energy value was used; the circles are the calculations for diffuse distribution with half of the two-proton separation energy value.

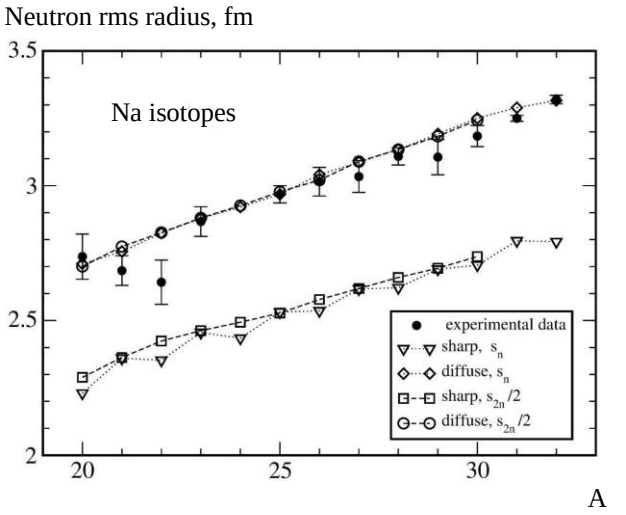

Fig. 2. Dependence of the effective rms radii for neutron spatial distributions in sodium isotopes on the mass number A. The black circles are the experimental data [14], the triangles are the calculations in the framework of the GT approach using one-neutron separation energy for neutron chemical potential; the squares are the calculations in the framework of the GT approach with half the two-neutron separation energy value; the rhombuses are the calculations for diffuse distribution with one-neutron separation energy; the circles are the calculations for diffuse distribution with half the two-neutron separation energy value.

As the charge number is fixed, the figure actually depicts the dependence on the number of neutrons $N = A - 11$. The triangles indicate the calculation in the framework of the GT approach for the sharp distribution (5) according to the formula (16). The rhombuses indicate the calculation using the direct variational method for the diffuse distribution (17) in accordance with the expression (25). In both cases, calculations were done using the experimental values of the one-proton separation energy s_p [15] for the proton chemical potential μ_p in accordance with (4). For clarity, the points are connected by dotted lines. As can be seen from the figure, the triangles are located much lower than the experimental data, while the rhombuses are almost identical to them. The difference between the upper and lower graphs is about of 0.5 fm. So, the account of the diffuse edge in the spatial distribution of protons increases the proton rms radii by about 20 %. The results of the calculation using half values of the two-particle nucleus separation energy $s_{2n}/2$ and $s_{2p}/2$ almost coincide with the calculations for single-nucleon separation energies. Here and below, we did not perform calculations for isotopes with no experimental data are available.

Fig. 2 shows the results of calculations of the neutron effective rms radii in sodium isotopes as a function of the mass number A together with the experimental data. For notations similar to those of Fig. 1 calculations were done using the one-neutron separation energy s_n [15] for the neutron chemical potential μ_n in accordance with (4). It is seen from Fig. 2 that the triangles are located below the experimental data by about of 0.5 fm. The rhombuses reproduce the experimental data fairly well and show the monotonous growth as the mass number increases. One should notice the sawtooth behavior for the calculation marked by triangles. This calculation corresponds to the one-neutron separation energy s_n taken for the neutron chemical potential. The sawtooth behavior disappears and the A-dependence of neutron rms radius becomes monotonous if we use the half-value of the two-neutron separation energy, $s_{2n}/2$, for the neutron chemical potential, see squares connected by the dashed line in Fig. 2. Such sawtooth dependence is a manifestation of the pairing effect which contributes to the single neutron separation energy s_n and cancels out in $s_{2n}/2$. The pairing effect is not that pronounced if the diffuse neutron distribution is used, the calculations using s_n (circles) and $s_{2n}/2$ (rhombuses) for the neutron chemical potential are practically coincided, see Fig. 2. It should be noted that in our model the pairing effects are manifested exclusively through the experimental values of one-particle neutron and proton

chemical potentials. We note, that the use of experimental values of s_q for chemical potentials still does not allow to reproduce well the fine structure of the mass number dependence of measured rms radii.

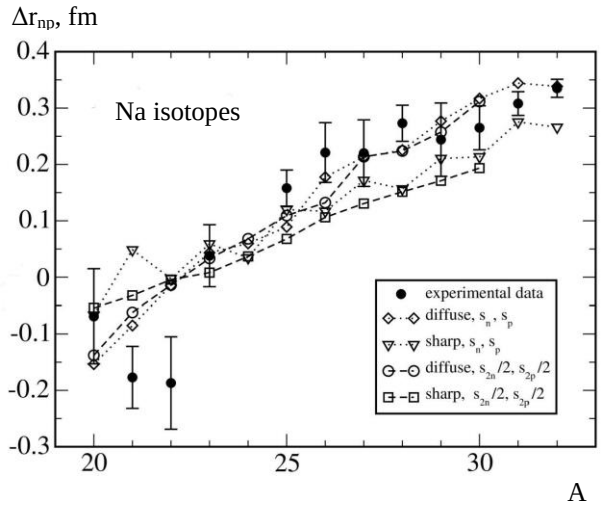

Fig. 3. Difference Δr_{np} between the effective rms radii of the neutron and proton spatial distributions as a function of A for Na isotopes. The notations are the same as in Figs. 1 and 2.

Figs. 3, 4, and 5 depict the calculation results for the difference between the neutron and proton rms radii

$$\Delta r_{np} = \sqrt{\langle r^2 \rangle_n} - \sqrt{\langle r^2 \rangle_p}$$

for Na, Sn, and Pb isotopes in comparison with the experimental data [16]. Fig. 3 shows the difference between Figs. 2 and 1. As seen from Fig. 3 the experimental data are described quite well with all four calculations presented. Although Figs. 1 and 2 show that step-like distributions underestimate the rms radii by an average of about 20 %, nevertheless, when calculating the difference, such shifts are mutually compensated. The diffuse distribution calculations demonstrate slightly steeper slopes than the stepped distribution calculations. This can be explained by the fact that for the diffuse distribution, the rms neutron radii increase more rapidly with the increase of the number of neutrons N than for the step-like distribution. The fine structure, however, is not reproduced, especially within the region of neutron-deficient isotopes. In general, the calculations with diffuse distribution are better to describe the experimental data.

In Figs. 4 and 5 there is a noticeable difference (of about 25 - 30 %) between two types of calculations which correspond to the diffuse and stepped nucleon distributions. The calculations for the diffuse nucleon distribution (marked as rhombuses) give a better description of the experimental data and are located higher than calculations for the stepped nucleon distribution (marked as triangles). In both Figs. 4 and 5 the sawtooth A-dependence is clearly seen for Δr_{np} obtained using single nucleon separation energies s_q. This indicates the pairing effect contribution to the isotopic difference in the root means square radii. The sawtooth dependence is eliminated by the use of the half-value of the experimental two-nucleon separation energies $s_{2n}/2$ and $s_{2p}/2$ for the corresponding chemical potentials, see squares and circles in Figs. 4 and 5.

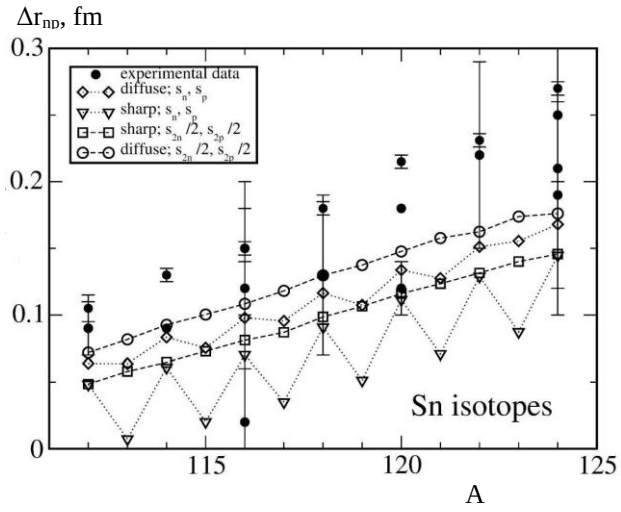

Fig. 4. Difference Δr_{np} between the rms radii of the neutron and proton spatial distributions as a function of A for Sn isotopes. The notations are the same as in Fig. 3. The experimental data were taken from Refs. [16 - 18].

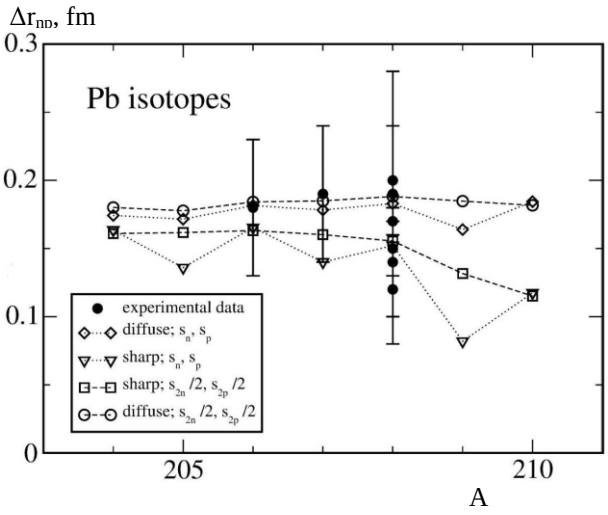

Fig. 5. Difference Δr_{np} between the rms radii of the neutron and proton spatial distributions as a function of A for Pb isotopes. The notations are the same as in Fig. 3. The experimental data were taken from Refs. [19 - 21].

The isotopic shift Δr_{np} between the neutron and proton rms radii (neutron skin) is presented in Fig. 6 as a function of the asymmetry parameter X for different nuclei. The experimental data (symbols with error bars) are taken from [16] where the isotopic difference between the rms radii was estimated as $\Delta r_{np} = (-0.04 \pm 0.03) + (1.01 \pm 0.15) X$. The result of this linear fit is presented by the dashed line in Fig. 6. Calculations shown in Fig. 6 were performed using one-particle separation energies for the sharp (triangles) and the diffuse (rhombuses) nucleon distributions. As seen from the figure, both types of calculations are mostly located within the limits of experimental errors. Fig. 7 shows similar calculations as in Fig. 6 except half the values of the two-particle separation energy are taken for the chemical potentials instead of the one-particle one to exclude the pairing effect.

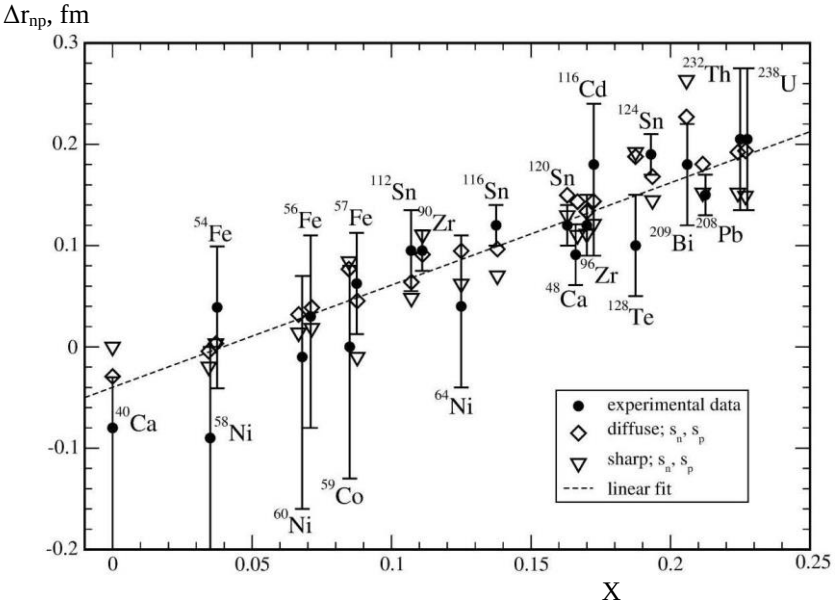

Fig. 6. Difference Δr_{np} between the rms radii of the neutron and proton spatial distributions as a function of the asymmetry parameter X for a set of nuclei. The experimental data are taken from [16], the dashed line is the linear approximation taken from [16], the triangles are the calculation in the framework of the GT approach, the rhombuses are the calculation for the diffuse distribution.

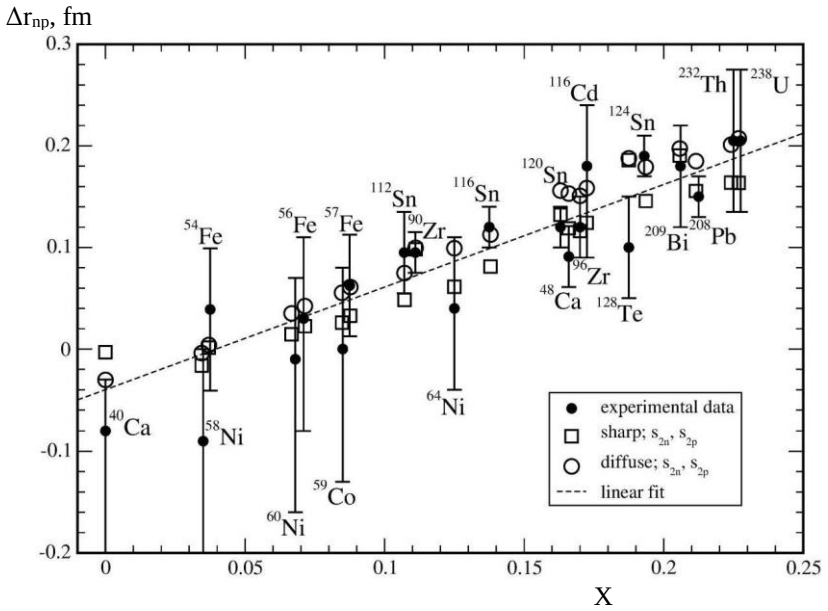

Fig. 7. Difference Δr_{np} between the rms radii of the neutron and proton spatial distributions as a function of the asymmetry parameter X for a set of nuclei. The experimental data are taken from [16], the dashed line is the linear approximation taken from [16], the squares are the calculation within the GT approach, the circles are the calculation for the diffuse distribution.

In contrast to the significant shift of about 0.5 fm in proton and neutron rms radii due to the presence of diffuse layer in spatial nucleon distribution (compare triangles and rhombuses, respectively, in Figs. 1 and 2), the contribution from the diffuse layer has an only slight effect on the isotopic shift Δr_{np} as can be concluded from Figs. 6 and 7 paying attention to the location difference between triangles and rhombuses in Fig. 6 and also between squares and circles in Fig. 7. The reason for the weak sensitivity of Δr_{np} on the presence of the diffuse layer is that the contributions to rms radii gained from the diffuse surface are partially canceled in the resulting isotopic difference. This justifies the application of simple nucleon distribution (5) in describing the properties of the neutron skin Δr_{np}.

4. Conclusions

In this paper, we have studied the influence of the diffuse surface of a nucleus on its rms radii and their difference by comparing the results of calculations for two cases. In the first case, in the framework of the Gibbs - Tolman approach, we considered the stepped spatial distribution of nucleons having formal equimolar radius located within the surface region of a nucleus. The bulk density was determined by adjusting the values of the chemical potentials to their experimental values using the nuclear matter equation of state. In the second case, the direct variational method was used applying a Fermi-like distribution function for the spatial distribution of nucleons. The neutron and proton densities in the center of a nucleus were normalized to the values obtained within the Gibbs - Tolman approach.

It is found that the use of the diffuse nucleon distribution gives a better description of the experimental rms radii as demonstrated in Figs. 1 and 2 for sodium isotopes. The contribution from the diffuse surface layer increases the neutron and proton rms radii by about 20 % as compared to the stepped nucleon distribution. For sodium isotopes, the neutron rms radius exhibits a monotonic increase with increasing mass number as seen from Fig. 2.

The isovector shift Δr_{np} between the neutron and proton rms radii was calculated for tin and lead isotopes using both the diffuse and stepped nucleon distributions. For both tin and led isotopes the use of diffuse Fermi-like distribution allows better reproduction of the experimental values Δr_{np}. The influence of the pairing effect on the isovector shift Δr_{np} is demonstrated in Figs. 3 and 4 for Sn and Pb isotopes. The sawtooth behavior of $\Delta r_{np}(A)$ reflects the odd-even effect in the one-nucleon separation energies s_q used for corresponding chemical potentials. After replacing the one-particle separation by the half-value of the two-particle separation energy the mentioned behavior disappears and practically monotonic dependence on the mass number is obtained for Δr_{np}. The calculations of the neutron skin for a certain set of nuclei, from light to heavy masses, depending on the asymmetry parameter, show that both models describe the experimental data within the experimental errors.

The work was supported in part by the Fundamental Research program “Fundamental research in high energy physics and nuclear physics (international collaboration)” at the Department of Nuclear Physics and Energy of the National Academy of Sciences of Ukraine.

REFERENCES

1. W.D. Myers. Geometric properties of leptodermous distributions with applications to nuclei. Nucl. Phys. A 204 (1973) 465.
2. C.J. Batty et al. Experimental Methods for Studying Nuclear Density Distributions. In: *Advances in Nuclear Physics*. Ed. by J.W. Negele and E. Vogt (New York: Plenum Press, 1989) Vol. 19, p. 1.
3. M. Warda et al. Analysis of bulk and surface contributions in the neutron skin of nuclei. Phys. Rev. C 81 (2010) 054309.
4. S.V. Lukyanov, A.I. Sanzhur. Neutron skin and halo in medium and heavy nuclei within the extended Thomas - Fermi theory. Nucl. Phys. At. Energy 17(1) (2016) 5.
5. J.W. Gibbs. In: *The Collected Works* (New York: Longmans, Green and Co., 1928) Vol. I, p. 219.
6. R.C. Tolman. The effect of droplet size on surface tension. J. Chem. Phys. 17(3) (1949) 333.
7. J.S. Rowlinson, B. Widom. *Molecular Theory of Capillarity* (Oxford: Clarendon Press, 1982).
8. V.M. Kolomietz, S.V. Lukyanov, A.I. Sanzhur. Curved and diffuse interface effects on the nuclear surface tension. Phys. Rev. C 86 (2012) 024304.
9. V.M. Kolomietz et al. Equation of state and radii of finite nuclei in the presence of a diffuse surface layer. Phys. Rev. C 95 (2017) 064305.
10. V.M. Kolomietz, S.V. Lukyanov, A.I. Sanzhur. Nucleon distribution in nuclei beyond the β-stability line. Phys. Rev. C 85 (2012) 034309.
11. V.M. Kolomietz, A.I. Sanzhur. Thin structure of β-stability line and symmetry energy. Int. Jour. Mod. Phys. E 22(1) (2013) 1350003.
12. V.M. Kolomietz, A.I. Sanzhur. Equation of state and symmetry energy within the stability valley. Eur. Phys. J. A 38 (2008) 345.

13. M. Brack, C. Guet, H.-B. Håkansson. Selfconsistent semiclassical description of average nuclear properties – a link between microscopic and macroscopic models. Phys. Rep. 123 (1985) 275.
14. T. Suzuki et al. Neutron skin in Na isotopes studied via their interaction cross sections. Phys. Rev. Lett. 75 (1995) 3241.
15. G. Audi et al. The Ame2012 atomic mass evaluation. (I). Evaluation of input data, adjustment procedures. Chin. Phys. C 36(12) (2012) 1287; M. Wang et al. The Ame2012 atomic mass evaluation. (II). Tables, graphs, and references. Chin. Phys. C 36(12) (2012) 1603.
16. A. Trzcińska et al. Neutron density distributions deduced from antiprotonic atoms. Phys. Rev. Lett. 87 (2001) 082501.
17. L. Ray. Neutron isotopic density differences deduced from 0.8 GeV polarized proton elastic scattering. Phys. Rev. C 19 (1979) 1855.
18. A. Krasznahorskay et al. Neutron-skin thickness in neutron-rich isotopes. Nucl. Phys. A 731 (2004) 224.
19. V.E. Starodubsky, N.M. Hintz. Extraction of neutron densities from elastic proton scattering by ^{206,207,208}Pb at 650 MeV. Phys. Rev. C 49 (1994) 2118.
20. S. Karataglidis et al. Discerning the neutron density distribution of ^{208}Pb from nucleon elastic scattering. Phys. Rev. C 65 (2002) 044306.
21. B.C. Clark, L.J. Kerr, S. Hama. Neutron densities from a global analysis of medium-energy proton-nucleus elastic scattering. Phys. Rev. C 67 (2003) 054605.

С. В. Лук'янов*, А. І. Санжур

Інститут ядерних досліджень НАН України, Київ, Україна

*Відповідальний автор: lukyanov@kinr.kiev.ua

ВПЛИВ ПОВЕРХНЕВИХ ЕФЕКТІВ НА НЕЙТРОННУ ШКІРУ В АТОМНИХ ЯДРАХ

Досліджено вплив дифузного поверхневого шару скінченного ядра на середньоквадратичні радіуси та їхній ізотопний зсув. Представлено розрахунки в рамках підходу Гіббса - Толмана з використанням експериментальних значень енергій відокремлення нуклонів. Результати порівнюються з розрахунками, отриманими за допомогою прямого варіаційного методу та пробних фермі-подібних функцій.

Ключові слова: нейтронна шкіра, наближення Гіббса - Толмана, прямий варіаційний метод, сили Скірма.

Надійшла/Received 14.11.2019